Original Article

Experimental validation of lift and drag forces on an asymmetrical hydrofoil for seafloor anchoring applications

Gerry Byrne[1] iD **, Tim Persoons[1]** iD **and William Kingston[2]**

Abstract

Tidal power can be described as harnessing the kinetic energy of the in and out flows known as tides created by the changing gravitational pull of the moon and the sun on the oceans of the world. As the relative positions of the sun and moon can be accurately predicted, so can the resultant tidal movements, making tidal energy such a valuable resource and an attractive option for renewable power generation. However, the high costs and difficulties associated with the deployment of underwater turbines, which includes anchoring, are prohibitive factors in the widespread utilisation of tidal power technology. Existing turbine fixation methods are primarily based on the use of large gravity anchors or monopole structures to secure the turbine to the seabed. In an effort to reduce size, environmental impact on the seafloor and installation cost, a hydrofoil-based anchor could be considered. The objective of this study is to experimentally test the lift and drag force behaviour of a finite-span hydrofoil with endplates, whose profile was selected based on simplified two-dimensional (2D) numerical simulations using the vortex panel method. A customised lift and drag force measurement system for this prototype hydrofoil was designed, fabricated and calibrated, and subsequently installed and tested in the Dutch Tidal Testing Centre (TTC) in Den Oever, the Netherlands. A series of tests with force and flow velocity measurements are described for different angles-of-attack under realistic tidal flow conditions. Results for the lift and drag coefficients as a function of angle-of-attack are compared to numerical simulation data and revealed that the real-world lift force is predicted well, whereas the drag force is underpredicted by the numerical predictions. These findings provide useful information for the design of anchoring systems based of hydrofoil profiles.

Introduction

There is a growing worldwide demand to switch to renewable energies for electricity generation primarily driven by concerns over climate change and the desire to lower dependency on fossil fuels. Tidal power electricity generation can be used to displace electricity, which would be otherwise generated by power plants fired by fossil fuels, thus reducing greenhouse gas emissions. Tidal power is an underdeveloped form of renewable energy, in which turbines or oscillating devices are placed in tidal streams to convert the kinetic energy into mechanical energy, which is then used to generate electricity. The energy density of

water allows large amounts of energy to be harnessed in relatively low-velocity flows. These flows are predictable and, although not always constant, they do not suffer the intermittency issues associated with wind energy.

The estimates of global potential of tidal energy generation vary, but it is widely agreed that tidal stream energy
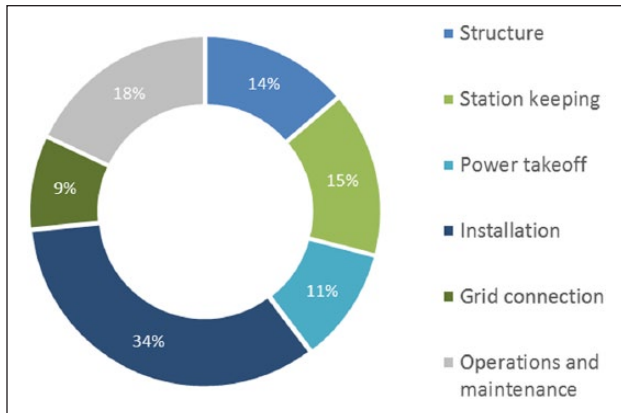
[1]School of Engineering, Trinity College Dublin, Dublin, Ireland
[2]Trinity Business School, Trinity College Dublin, Dublin, Ireland

Corresponding author:
Tim Persoons, School of Engineering, Trinity College Dublin, Parsons Building, Dublin 2, Ireland.
Email: tim.persoons@tcd.ie

Figure 1. Breakdown of costs associated with the operation (light grey segment, 18%) and installation (coloured segments, totalling 82%) of tidal stream energy generators.
Source: Adapted from The Carbon Trust (2011).

capacity could exceed 120 GW globally. It has been estimated that tidal stream energy could theoretically supply more than 150 TW/h per annum, well in excess of all domestic electricity consumption in the United Kingdom. This represents a potential total global market size of up to 90 GW of generating capacity. The UK's tidal power resource is estimated to be more than 10 GW, representing about 50% of Europe's tidal energy capacity (Tidal Energy Today, 2015). In Ireland, the theoretical gross energy content in waters between the 10 m depth contour and the 12 nautical mile territorial limit is 230 TWh/year (Sustainable Energy Ireland, 2007).

However, despite the relative abundance of this predictable energy resource, the cost of harnessing it has proved prohibitive. The Carbon Trust estimates the present cost of tidal stream energy based on projects of around 10 MW at 33–37 p/kWh (The Carbon Trust, 2011), which is considerably more than current electricity prices for non-domestic use at approximately 11 p/kWh (SI Ocean, 2013). This high cost is a major obstacle to the development of tidal stream energy. As shown in Figure 1, installation costs (at 34%) are the single biggest expenditure over the lifetime of a tidal stream device. Therefore, one method of reducing the cost of tidal energy is to reduce those associated installation costs (SI Ocean, 2013).

SI Ocean (2013) states that installation accounts for 27% of the lifetime costs of a tidal array and that a change of design and/or installation method would clearly impact on overall costs. The Carbon Trust also sees innovation play a key role in reducing energy costs (United Kingdom Department for Business, Energy & Industrial Strategy, 2017). Developing experience and large-scale projects are part of the natural progression of any industry. Developing innovative designs is one of the recommendations that have potential to reduce the cost of tidal stream energy devices.

In a step towards significantly reducing the installation costs of tidal energy devices, the hypothesis that an asymmetrical hydrofoil could be used to help fixate a tidal stream

device to the seabed was investigated. This hypothesis is based on a patent by Kingston (2012). This patent describes a hydrofoil-based anchor which fixates to the seafloor by means of a plug-and-socket connection, where the plug (on the bottom of the hydrofoil anchor) is held into the socket by means of the negative (downward) lift force generated by the asymmetrical hydrofoil in response to tidal streams (Kingston, 2012). The lift force substitutes the weight of a gravity anchor in holding the plug-and-socket connection firmly on the seafloor. It is thought that by utilising the negative lift or down force generated by an asymmetrical hydrofoil, the scale and, therefore, the cost of the foundations needed to secure a tidal stream energy extraction device could be dramatically reduced. A feature of this invention is a hydrofoil which is compact during deployment, but whose wingspan can be expanded when it is in position.

The objective of this article is to describe the design and experimental validation testing of a prototype hydrofoil mounted on a custom-built test apparatus with an adjustable angle-of-attack, suitable for use in a tidal test facility. The aim is to verify to what extent the lift and drag coefficient behaviour (in terms of absolute values and trends) of the hydrofoil predicted by basic 2D numerical simulations corresponds to the real-world behaviour for a finite-span hydrofoil with endplates under realistic tidal flow conditions. The limitations of numerical predictions and the potential risks of the absence of experimental validation will be emphasised.

Not within the scope of this study is the design of the hydrofoil anchoring structure itself. For such a future hydrofoil-based anchoring system, although the hydrofoil profile shape could remain the same, the foil itself would need to be scaled up or multiple foils would be combined onto a single support structure to generate sufficient (downward) lift force to hold the device to be anchored. The study reported on in this article constitutes the first step towards a design of the hydrofoil-based anchoring system (Kingston (2012)).

## Description of the experimental hydrofoil test apparatus

Hydrofoil selection

While hydrofoils are not a new concept, most existing hydrofoil applications are for high-speed naval applications. As such, these are typically high aspect ratio hydrofoils, which are optimised to provide stable lift in high-velocity operation. Unfortunately, tidal flows are of much lower velocity, typically about 2–3 m/s flow velocity at most. The ideal hydrofoil profile for use in this application has the following:

- A high lift/drag ratio at high angles-of-attack.
- Delayed and predictable stall behaviour at high angles-of-attack.
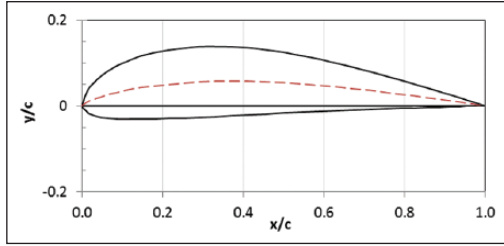
Figure 2. Göttingen (GOE) 527 hydrofoil profile shape with maximum thickness $t/c = 16.5\%$ at 29.5% chord, maximum camber $h/c = 5.8\%$ at 39.5% chord (Kingston (2012)).
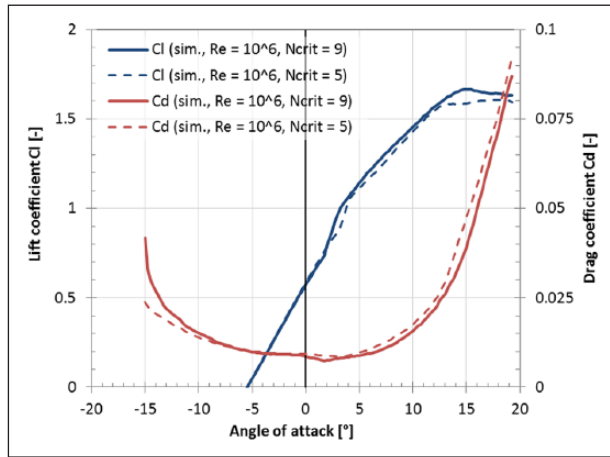
Figure 3. Göttingen (GOE) 527 lift and drag coefficient curves, obtained using numerical simulation for $Re = 1,000,000$ and $N_{crit} = 9$ (solid lines) and $N_{crit} = 5$ (dashed lines) (Kingston (2012)).

- A thick cross section to better resist spanwise structural loads.
- Have predictable behaviour in high Reynolds number flows.
- Have an easy-to-manufacture profile.

The Göttingen 527 (GOE527) profile was selected as best meeting the above specifications. It is an asymmetrical profile with maximum camber of $h/c = 5.8\%$ of the chord length c, chosen from the UIUC aerofoil profile database. Figure 2 shows the profile shape in dimensionless coordinates, normalised by the chord length c. Note that the profile is shown in the conventional position in Figure 2, while it will be used upside down for the tests, with positive lift force in the downwards direction, as shown in Figure 5.

The GOE527 profile was selected through a comparison of profiles using the airfoiltools database (Airfoil Tools, n.d.). The airfoiltools database was compiled using theoretical calculations using the Xfoil program, which has been validated as sufficiently accurate profile data (Batten et al., 2007). Xfoil is a numerical simulation package originally developed by Drela (1989). At its core,

Xfoil uses a high-order vortex panel solver (Katz, 2010) with a fully coupled viscous/inviscid interaction method (Drela and Giles, 1987). Figure 3 shows the lift and drag coefficients of the GOE527 profile as a function of angle-of-attack, as calculated by Xfoil. The data represent a flow with Reynolds number $Re = 1,000,000$ and two values of the Xfoil parameter N_{crit} which describe the transition behaviour. A value $N_{crit} = 9$ (solid lines in Figure 3) is representative of turbulence intensity values encountered in a typical wind tunnel environment. A lower value $N_{crit} = 5$ (dashed lines in Figure 3) represents higher turbulence intensity values, such as those encountered in a poorly designed wind tunnel (Kingston (2012)). In the remainder of this article, a value of $N_{crit} = 9$ will be assumed.

As shown in Figure 3, the lift and drag curves exhibit a high lift/drag ratio and predictable stall behaviour. It has a maximum thickness of $t/c = 16.5\%$ of the chord length c, which was the highest of all profiles considered for this study. Although thicker profiles are used as hydrofoils, for instance, as ship rudders where a thickness of 20% is required to absorb high structural loads, 16.5% was deemed adequate for this experimental study. It balances good structural rigidity with a lightweight and portable design which could be manufactured at a reasonable cost.

An asymmetric cambered profile was selected instead of a symmetric $(h = 0)$ profile for two main reasons: (1) the GOE527 profile has a relatively flat pressure surface, making it relatively easy to manufacture; and (2) the cambered hydrofoil yields a non-zero lift force even at zero angle-of-attack, as appropriate for the target application of seafloor anchoring.

It should be noted that Xfoil assumes 2D flow, which does not account for three-dimensional (3D) effects which occur inevitably in finite-span hydrofoils, induced by pressure imbalances at the ends (wing tips). This particularly affects short hydrofoils. However, end effects in this study have been partially mitigated using endplates to reduce tip vortices, as described in the following section.

Design of the hydrofoil test apparatus

The hydrofoil test device consisted of a hydrofoil (wingspan $b = 1.4$ m, chord length $c = 0.57$ m and aspect ratio $AR = b/c = 2.46$) with two rounded endplates (see detailed description below), supported by two mounting arms with an integrated lift and drag sensing system. Figure 4 shows a schematic diagram of the mounting frame, which is fitted with a circular flange for attaching to a corresponding flange on an existing test beam (shown in red in Figure 4), already installed in the tidal testing facility[1] (see section 'Hydrofoil testing methodology'). A removable lifting arm is fitted to aid installation.

Four ribs with the selected hydrofoil profile were plasma cut out of 10-mm-thick steel plate; in each rib, four
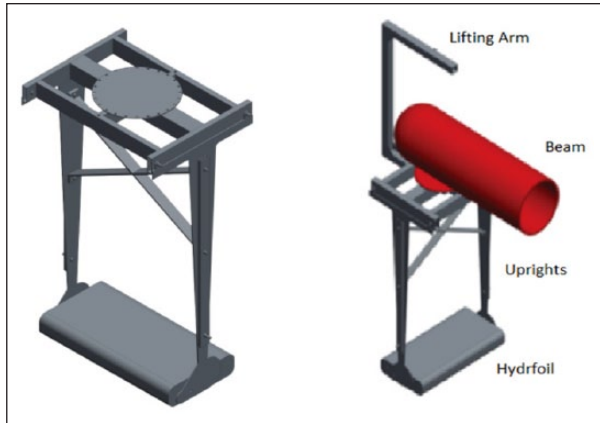
Figure 4. Hydrofoil test apparatus, to be mounted to existing beam (shown in red) installed in the Tidal Testing Centre facility (see also Figure 9).
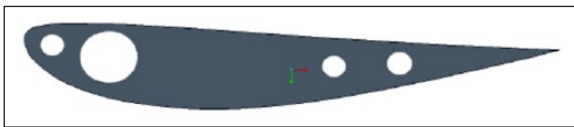
Figure 5. Schematic view of a single rib showing the hydrofoil profile structure.

circular holes were cut to allow the ribs to be welded onto spanwise tubular steel spars (Figure 5). The central spar is 60.3 mm diameter and the three smaller are 26.9 mm diameter, each $b = 1.4$ m long . A 4-mm-thick steel skin is bent around the plates using a computer numerically controlled (CNC) rolling machine and welded into place. Two 770 mm × 200 mm × 5 mm endplates are welded to both hydrofoil tips. Two M25 mm threaded holes were machined into the hydrofoil endplates to allow attachment to the supporting arms. The hydrofoil test apparatus was manufactured by Arklow Marine Services (AMS).[2]

Relative to the profile thickness $(t = 0.094$ m$)$, the endplates are $2.13t$ m high and extend a distance of $1.06t$ past both the leading edge and trailing edge of the hydrofoil, as can be seen in Figure 6. These endplates serve two purposes: (1) to provide structural stability and facilitate fastening the hydrofoil at a given angle-of-attack onto the mounting arms, and (2) to reduce the hydrodynamic end effects associated with the pressure imbalance between pressure and suction surfaces of the hydrofoil. The latter effect causes tip vortices in 3D hydrofoil flows, which cause an increased downwash and effective reduction in the apparent angle-of-attack, thereby reducing lift and increasing drag force on a finite-span hydrofoil compared to an infinite-span hydrofoil with the same profile. The endplates thus play an important role in partly mitigating against this loss of lift force, similar to winglets on modern commercial passenger aircraft (Kuethe and Chow, 1998; Munson et al., 2013).

Figure 6. Hydrofoil during fabrication in Arklow Marine Services (see Note 2).

## *Hydrofoil lift and drag force measurement approach*

Figure 7(a) and (b) shows a schematic diagram of the hydrofoil mounting frame in place in the tidal testing facility (see Note 1) (see section 'Hydrofoil testing methodology'), with the definition of positive lift force, drag force and angle-of-attack. The immersion depth D is 1.5 m from the water surface to the pressure surface of the hydrofoil. The immersion depth did not vary by more than 5% for the investigated range of angle-of-attack and flow velocity. As indicated in Figure 7(b), the endplates and supporting arms are 10 mm thick for minimal flow blockage in the vicinity of the hydrofoil, yet the supports increase to a thickness of 50 mm at a distance of $5t$ (0.47 m) above the hydrofoil to ensure sufficient rigidity, a prerequisite of the test facility as described in more detail in section 'Experimental results and discussion'.

Eight strain gauges are used to achieve independent measurements of the lift force and drag force imparted on the hydrofoil. Two sets of four strain gauges (1D, 120 Ω) are located on either side of one mounting arm, in a pattern shown in Figure 7(c). These are wired up in two Wheatstone bridges. The signals are read into a National Instruments 9219 24-bit 4-channel input module. The gauge factor equals 2.1 at 20°C and has a positive temperature coefficient of 0.0263%/K. The sensors were calibrated prior to testing, resulting in the calibration curves shown in Figure 8. The crosstalk between lift and drag sensors does not exceed 3%. In actual measurement conditions, the estimated uncertainty based on a 95% confidence level is ±5.1 kg (±3.2% at an angle-of-attack of 3°) for the lift force sensor and ±1.0 kg (±2.6% at an angle-of-attack of 3°) for the drag force sensor, as described in more detail in Appendix 2.
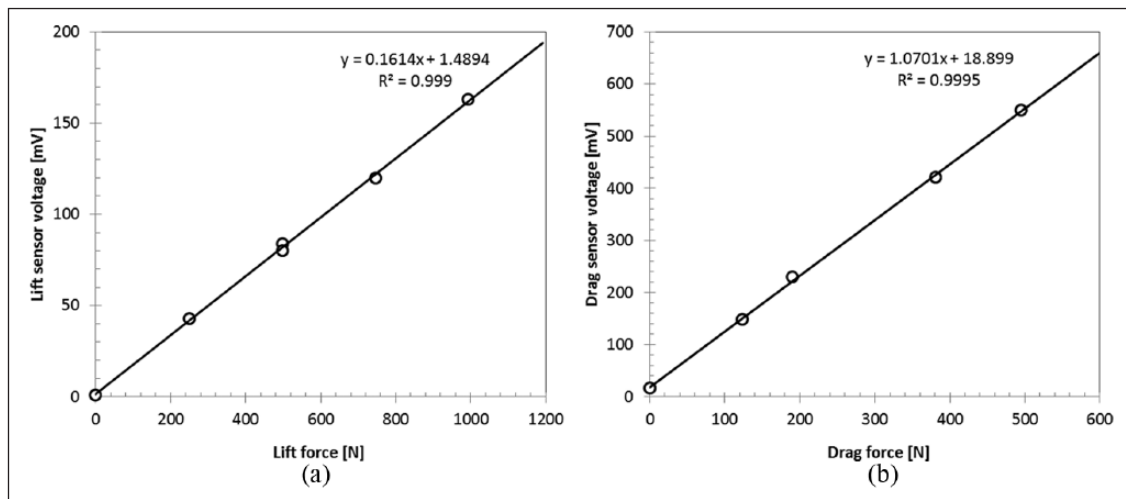
Hydrofoil testing methodology

Funding was granted by the Marine Renewables Infrastructure Network (MARINET) under Framework
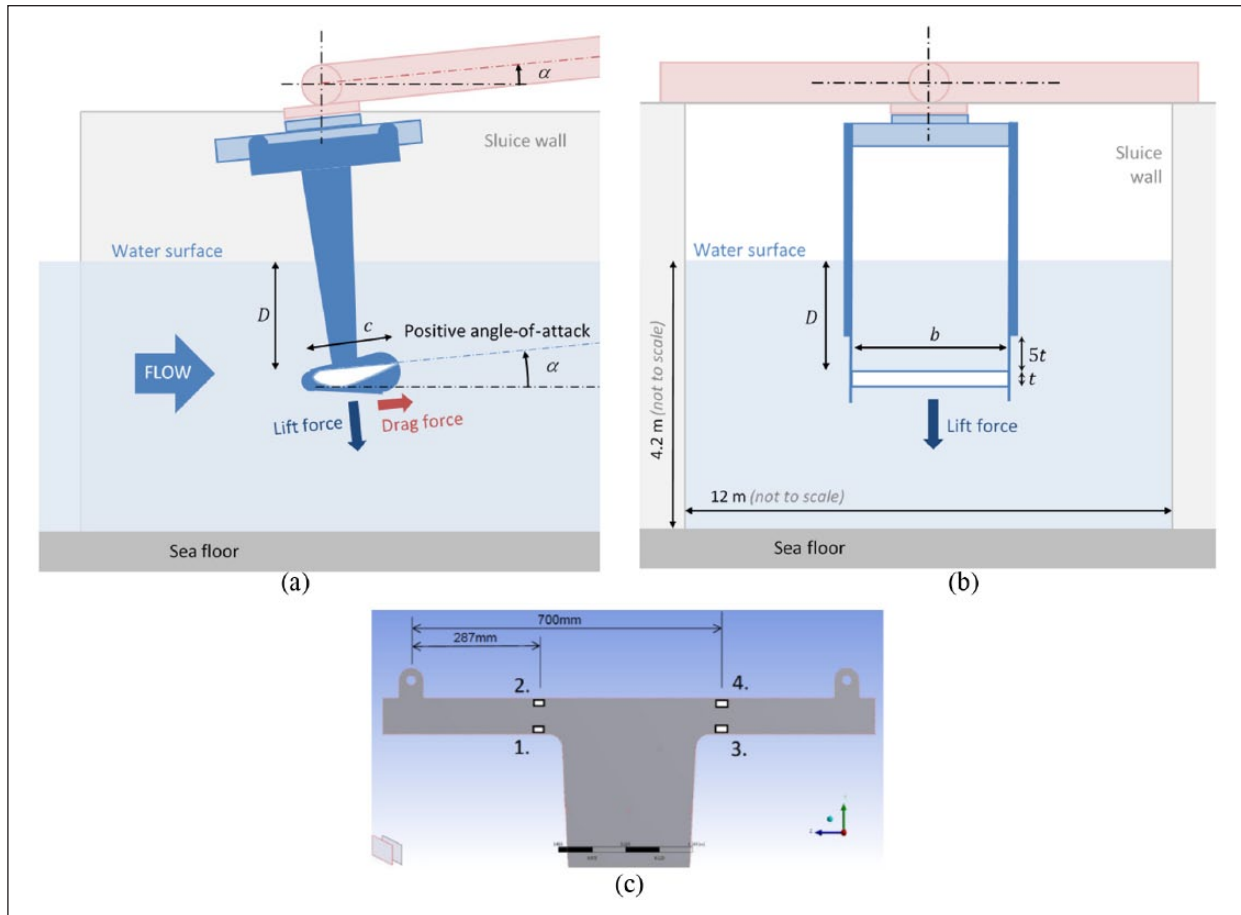
Figure 7. (a, b) Hydrofoil geometry and lift and drag force definition (note: schematics are not drawn to scale) and (c) strain gauges layout on the hydrofoil mounting arms.

Figure 8. (a) Lift and (b) drag force calibration curves.

Programme 7 (FP7) to carry out testing at the Den Oever Tidal Testing Centre facility in the Netherlands (See Note 1). This facility consists of a 12-m wide and 4.2-m deep sluice, which discharges water from the fresh water Lake IJsselmeer to the salt water Waddenzee. Water is discharged twice a day at accurately predictable flow rates of with flow velocities in the sluice of 1.5–4.5 m/s. The flow rate is predictable yet depends on the hydraulic head

in the lake. Thus, it depends on the amount of rainfall in previous days and it cannot be controlled. Typical flow velocity values are between 1.5 and 2.5 m/s, whereas a flow velocity greater than 3 m/s only occurs at very low tides and a lot of rainfall. When the sluice gate is closed, there is no flow allowing easy positioning of the hydrofoil in the flow. The walls of the sluice gate are concrete blocks as is the base. Permission was given by turbine manufacturing company Tocardo[3] to use a T-shaped mounting beam already in place on site (Figure 9).

Once installed, the hydrofoil angle-of-attack α could be changed by raising or lowering the centre leg of the mounting beam (see Figure 7(a)), utilising a hoist attached to the wall. The velocity of the tidal stream was measured using an acoustic Doppler current probe (ADCP) submerged to the same immersion depth $D = 1.5$ m as the hydrofoil, a few metres downstream from the hydrofoil with the measurement volume adjacent to but at the same depth D as the hydrofoil. A computer-controlled data acquisition system was used to collect the data from the strain gauges and ADCP in real time, throughout several consecutive tidal stream periods. Tests were carried out over a 3-day period for a range of angles-of-attack is $-2.5° \leq \alpha \leq +11.4°$, with each test typically running for 4 hours at a time, 2 hours on either sides of peak low tide.

Figure 9. Test apparatus (grey, shown on left) fitted to Tocardo (See Note 3) beam (red) at TTC (See Note 1).

Experimental results and discussion

Using the calibration curves and a simple correction for the angle of the lift and drag sensors, the actual lift and drag forces on the hydrofoil could be determined. Readings for the drag force are corrected for the drag of the support arms and cross-brace by assuming the hydrofoil drag coefficient at zero angle-of-attack equals 0.009, based on the numerical predictions (see Figure 3). The effect of self-weight at different angles has been corrected for in the lift and drag force readings. Finally, the lift force reading has been corrected for the force exerted on the mounting frame by representing it as a simple flat plate of the same dimensions.

Table 1 shows a summary of the lift and drag coefficient results at the maximum flow velocity, which varied slightly between tidal cycles (depending on water heights, wind speed and direction) between 1.8 and 2.4 m/s. The corresponding peak Reynolds number based on hydrofoil chord length ($c = 0.57$ m) for each tidal cycle thus varied between $Re = 1,001,000$ and $Re = 1,359,000$. This Reynolds number range corresponds reasonably well with the Reynolds number for the Xfoil numerical simulation data ($Re_{sim} = 1,000,000$) shown in Figure 3. The difference in peak Reynolds number is considered small enough to permit the values to be plotted on a single chart in Figure 10.

Although the flow velocity varies during the tidal cycle, the velocity remains within 5% of the maximum velocity for approximately 30 minutes in each cycle, as can be seen in the sample measurement result shown in Figure 11. Therefore, the flow can be assumed quasi-steady at all times, and enough time is available to acquire sufficient independent samples. Measurements are recorded at 4 second intervals.

The experimental results are shown as markers in Figure 10, compared to the solid lines representing the numerical simulation results for this hydrofoil profile (GOE 527).

Figure 10 demonstrates a satisfactory agreement for the lift coefficient between the experiments and numerical simulations for a wide range of angle-of-attack ($-2.5° \leq \alpha \leq 8°$), although the highest angle-of-attack investigated ($\alpha = 11.4°$) shows a measured lift coefficient which is 15% higher than predicted numerically. The measured drag coefficient values

Table 1. Experimental results for the lift and drag coefficients at maximum flow velocity, corresponding to a Reynolds number Re between $1,001,000$ and $1,359,000$.

Hydrofoil angle-of-attack α (°)	−2.5	0.0	3.0	8.0	11.4
Maximum flow velocity (m/s)	2.0	1.8	2.0	2.1	2.4
Net downwards force (uncorrected) (kg)	69	86	153	243	471
Net streamwise force (uncorrected) (kg)	18	18	35	(74)[a]	(89)[a]
Lift coefficient (corrected), C_L	0.377	0.571	0.860	1.196	1.838
Drag coefficient (corrected), C_D	0.009	0.006	0.047	0.151	0.386
Lift-to-drag coefficient ratio, C_L / C_D	44.1	92.6	18.5	7.9	4.8

[a]The drag force sensor began failing intermittently immediately before these tests commenced; these readings should, therefore, be treated with care.
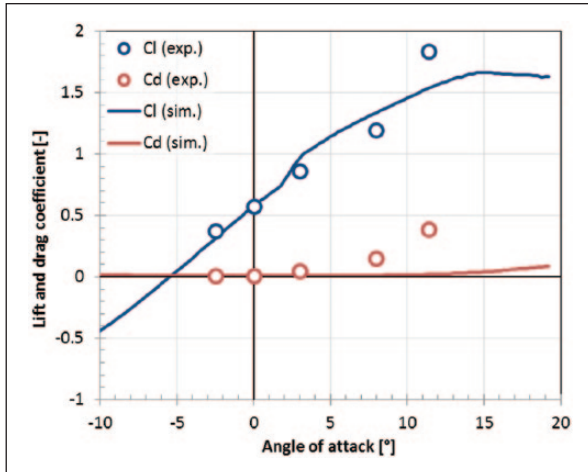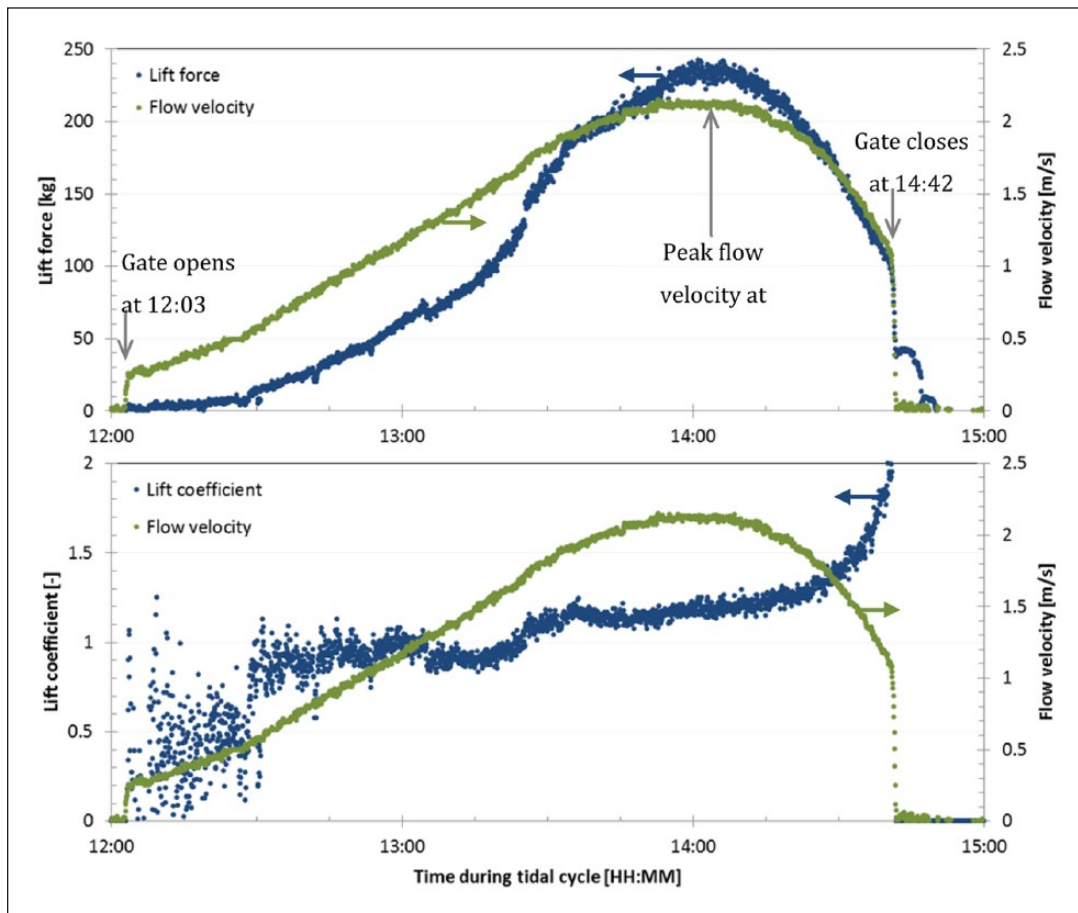
Figure 10. Hydrofoil lift and drag coefficient curves; solid lines represent numerical simulation results for the 2D hydrofoil ($Re = 1,000,000$; $N_{crit} = 9$) (Kingston (2012)) and the markers represent the experimental measurement results for the finite-span hydrofoil in the TTC (See Note 1) ($Re = 1,001,000 - 1,359,000$) (see Table 1).

show a reasonable agreement with the numerical predictions only at a small angle-of-attack $(-2.5° \leq \alpha \leq 3°)$. For the higher angles $(\alpha = 8°$ to $11.4°)$, the measured drag is an order of magnitude higher than the numerical prediction.

First, before assessing the agreement between the experimental and numerical data in earnest, it should be noted that although the physical shape of the hydrofoil profile has been fabricated to be as close as possible to the GOE 527 profile, the match is not perfect due to manufacturing constraints. For instance, the slight inward curvature on the trailing edge of the pressure side of the profile (shown in Figure 2 at location $x/c \cong 0.8$) proved difficult to reproduce faithfully even by CNC rolling and subsequently welding the steel skin plate, so this is simplified to a flat section on the fabricated hydrofoil.

Second, an important limitation to the validity of a comparison between the experimental and numerical results should be restated here: the hydrofoil in this experiment has a small span-to-chord length ratio $(AR = 2.46)$. By contrast, the Xfoil numerical simulation assumes an infinitely long wing profile $(AR \rightarrow \infty)$ with a purely 2D

Figure 11. Hydrofoil lift force, lift coefficient and flow velocity as a function of time, during one tidal ebb cycle, for a fixed hydrofoil angle-of-attack of $\alpha = 8°$. The values at peak flow velocity (at 14:05) correspond to the values for $\alpha = 8°$ in Table 1.

flow. The pressure difference between pressure (top) and suction (bottom) side of a finite-span hydrofoil causes leakage of fluid around the tips, which leads to 3D flow in the form of wing tip vortices. While in a normal lift-generating scenario, this would create a downwash, because of the inverted orientation in the case of the downwards lift-generating hydrofoil, an additional up-wash is created downstream of the hydrofoil. This vertical up-wash velocity component acts to reduce the effective angle-of-attack α_i experienced by the hydrofoil. As a result of the lift vector $\bar{L}$ tilting by the angle α_i, an induced drag force is created with magnitude $D_i = L\sin\alpha_i$. Assuming an elliptical distribution of the lift force along the spanwise direction, one can derive that $\alpha_i = C_l / \pi AR$ and the induced drag coefficient $C_{d,i} = C_l^2 / \pi AR$ (Kuethe and Chow, 1998). Therefore, this 3D flow effect is more pronounced at high angle-of-attack and for small aspect ratio hydrofoils, such as the one used in this study. Since the effective angle-of-attack reduces to $\alpha - \alpha_i$ (compared to α for an equivalent hydrofoil of infinite span), the effective lift force is expected to decrease for a finite hydrofoil compared to a value predicted for an infinite hydrofoil.

To help counteract the formation of wing tip vortices, the hydrofoil is equipped with two endplates, as described in section 'Hydrofoil selection', which help to compensate for the loss of lift. Since the measured lift coefficient is comparable to the Xfoil prediction in Figure 10, it can be reasonably assumed that the endplates have the intended effect of minimising wing tip vortex formation.

With regard to the drag coefficient data, the discrepancy between the higher experimental and lower numerical drag coefficient at high angle-of-attack can be partly attributed to the fact that numerical simulations tend to underestimate flow separation and the associated losses. Instead of the Xfoil methodology, computational fluid dynamics (CFD) simulations with finite volume discretisation and an appropriately selected turbulence model could be employed; however, this was outside the scope of this study.

Furthermore, the supporting arms had to be reinforced to satisfy concerns from the Dutch Ministry of Infrastructure and the Environment (Rijkswaterstaat)[4] concerning the mechanical strength of the original designs, which only featured 10-mm-thick mounting arms so as to minimise flow blockage effects at the ends of the hydrofoil. The reinforced arms include a $40\,\text{mm} \times 60\,\text{mm}$ hollow steel profile on the outside to increase lateral rigidity, thereby increasing the resonance frequency to $20\,\text{Hz}$ (see Appendix 3). The mounting arms thus form a 50-mm-wide bluff body in the flow, causing a significant turbulent wake to be formed. However, the steel profiles end $0.47\,\text{m}$ above the hydrofoil, leaving the final $0.47\,\text{m}$ $(=5t)$ length of supporting arms only $10\,\text{mm}$ thick, thereby reducing the bluff body blockage effect near the hydrofoil. Nevertheless, these turbulent wakes may still act to destabilise the flow across the hydrofoil, potentially causing a greater increase in drag than might have been the case for more slender supporting arms.

Figure 11 shows the time evolution of the lift force and flow velocity during one of these experiments, where detailed velocity information was available from the ADCP probe. As expected, the instantaneous lift coefficient (red markers in Figure 11) shows a near constant value from about 30 minutes before until 30 minutes after the moment of peak velocity, even though the velocity magnitude changes between about 1.5 and 2.2 m/s during that time period. The, respectively, lower and higher lift coefficient values during the acceleration and deceleration phases can be partly attributed to the fact that the velocity profile approaching the sluice is different. This may be compounded by the water level in the lake dropping slightly during the cycle, although the immersion depth of the hydrofoil below the surface never varied by more than $\pm 0.075\,\text{m}$ from an average depth $D = 1.5\,\text{m}$. The turbulence intensity was not measured, but this could also be different towards the beginning and end of the cycle.

As Figure 11 shows, the lift coefficient is reasonably independent of flow velocity during the majority of the tidal cycle. These findings can now be used in a thought experiment, to estimate the required size of a hydrofoil of this shape (GOE 527 with endplates and an aspect ratio of 2.46) to exert the same holding force as an equivalent gravity anchor consisting of a concrete block on a typical seabed. For a concrete gravity anchor with mass $M_{ga} = 2000\,\text{kg}$, $\rho_{ga} = 2400\,\text{kg/m}^3$ and water density $\rho = 1000\,\text{kg/m}^3$, the maximum horizontal anchoring force is $F_{ga} = \mu M_{ga} g(\rho_{ga} - \rho) / \rho$. In this expression, μ is the friction coefficient between the anchor base and the seabed, and g is the gravitational acceleration. Assuming a coefficient of friction $\mu = 0.6$ which is applicable to smooth concrete or rough steel on cohesionless sand soils (Thompson and Beasley, 2012), a 2000-kg concrete gravity anchor can hold a maximum of $F_{ga} = 16.5\,\text{kN}$ or $1680\,\text{kg-force}$.

The drag force on the system being anchored can be assumed to scale with the square of the tidal stream flow velocity, $F_s = C_{d,s} A_s (\rho U^2 / 2)$ – where $C_{d,s}$ and A_s represent the drag coefficient and area of the system being anchored. The gravity anchor should be designed with a minimum safety factor (arbitrarily, $SF = 2$) thus the maximum allowable system drag $F_{s,max} = F_{ga} / SF_{min} = 8.2\,\text{kN}$. For an arbitrary maximum flow velocity $U_{max} = 4\,\text{m/s}$, the product of system drag coefficient and area for this case would thus be $C_{d,s} A_s = 1.03\,\text{m}^2$. Since the holding force F_s varies with U^2, the gravity anchor is inevitably overdesigned for any lower flow velocity U≤Umax, with an effective safety factor given by equation (1)

$$SF_{eff,ga}(U) = \frac{F_{ga}}{C_{d,s} A_s \rho U^2 / 2} \qquad (1)$$

By contrast, downwards lift force L_{hf} of a hydrofoil-based anchor would increase with U^2. The required size of a hydrofoil with the same shape as the one investigated

here can be calculated using equation (2) and the assumption that the hydrofoil is mounted on a support structure resting on the seabed with a rough steel base of a similar footprint to the gravity anchor. Thus, $\mu L_{hf} = F_{ga}$

$$L_{hf} = C_{l,hf} A_{hf} \frac{\rho U^2}{2} \qquad (2)$$

Conservatively taking the lift coefficient at a moderate angle-of-attack of 3° equals $C_{l,hf} = 0.86$ (see Table 1). The required hydrofoil area to achieve a comparable holding force as the gravity anchor at maximum flow velocity thereby becomes $A_{hf} = (M_{ga}g(\rho_{ga} - \rho) / \rho) / (C_{l,hf} \rho U_{max}^2 / 2) = 3.99 \text{ m}^2$.

Since the tested hydrofoil has a planform area of $bc = 1.4 \cdot 0.57 = 0.80 \text{ m}^2$, a fivefold larger area would be required, or a linear scaling factor of 2.2. Thus, a single hydrofoil with chord length $c = 1.27 \text{ m}$ and span $b = 3.1 \text{ m}$ would generate the same holding force as a 2000-kg concrete gravity anchor in a 4 m/s flow velocity. Alternatively, multiple smaller hydrofoils could be combined on a single structure; however, this would require further analysis to study their interaction. The hydrofoil anchor would have a constant effective safety factor, independent of flow velocity

$$SF_{eff,hf}(U) = \frac{\mu L_{hf}}{\dfrac{C_{d,s} A_s \rho U^2}{2}} = \frac{\mu C_{l,hf} A_{hf}}{C_{d,s} A_s} = SF(=2) \qquad (3)$$

Figure 12 shows the effective safety factors for both anchor types in this example, as well as their holding force, as a function of tidal stream velocity U.

Admittedly, the above calculation simplifies the problem considerably and ignores any effects of the support structure; however, it does demonstrate the potential for hydrofoil-based anchor systems, as was also suggested by other researchers (Owen, 2007).

Summary and outlook

In summary, the tests that were carried out have given experimental evidence for the lift and drag forces on a finite asymmetrical hydrofoil with endplates. The main conclusion is that the lift force can be reasonably well predicted by 2D numerical simulations based on the vortex panel method (using Xfoil), but the drag force is underestimated by the numerical simulations. This is important information, which is crucial for the design of anchoring systems based on these hydrofoil profiles. Equally, this article clearly shows the limitations of Xfoil in relation to lift and drag force predictions, and the potential risks in relying on these predictions without adequate experimental validation in real-world flow conditions.
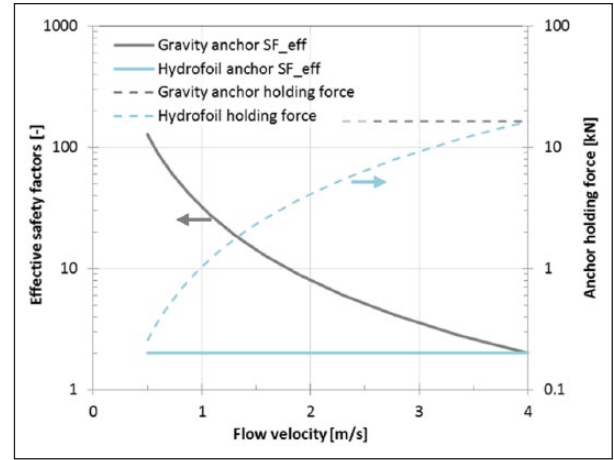
Figure 12. Sample comparison of a 2000-kg concrete gravity anchor on a sandy seabed and a hydrofoil anchor ($A_{hf} = 3.99 \text{ m}^2$, GOE 527 with endplates, $AR = 2.46$) in terms of effective safety factor SF_{eff} (solid lines, see equations (1) and (3)) and holding force (dashed lines) as a function of flow velocity.

If properly designed, hydrofoil anchoring systems could significantly reduce the costs associated with the deployment and retrieval of tidal flow anchoring due to the weight and size reduction capabilities. This cost reduction should assist in reducing the overall cost of energy from tidal streams and thus narrow the gap between this renewable resource and energy derived from fossil fuels.

Notes

1. Dutch Marine Energy Centre (DMEC), Den Oever, the Netherlands (https://www.dutchmarineenergy.com/dutch-test-facilities/tidal-technology/dmec).

2. Arklow Marine Services, Arklow, Co. Wicklow, Ireland (http://www.arklowmarine.ie/).
3. Tocardo International BV (http://www.tocardo.com).
4. http://www.rijkswaterstaat.nl/english.

ORCID iDs

Gerry Byrne https://orcid.org/0000-0002-4654-3276
Tim Persoons https://orcid.org/0000-0001-7215-4381

References

Airfoil Tools (n.d.) Specifications of the Gottingen 527 Airfoil. Available at: http://airfoiltools.com/airfoil/details?airfoil=goe527-il (accessed 17 December 2013).

Batten WMJ, Bahaj AS, Molland AF, et al. (2007) Experimentally validated numerical method for the hydrodynamic design of horizontal axis turbines. *Ocean Engineering* 34(7): 1013–1020.

Drela M (1989) XFOIL: An analysis and design system for low Reynolds number airfoils. In: Mueller TJ (ed.) *Low Reynolds Number Aerodynamics, Lecture Notes in Engineering*, vol. 54. Berlin: Springer, pp. 1–12.

Drela M and Giles MB (1987) Viscous-inviscid analysis of transonic and low Reynolds number airfoils. *AIAA Journal* 25(10): 1347–1355.

Katz J (2010) *Introductory Fluid Mechanics*. New York: Cambridge University Press.

Kingston W (2012) *Tideway anchor system*. US Patent 8215871 B2.

Kuethe AM and Chow CY (1998). *Foundations of Aerodynamics: Bases of Aerodynamic Design*. 5th ed. Hoboken, NJ: John Wiley & Sons.

Munson BR, Okiishi TH, Huebsch WW, et al. (2013) *Fundamentals of Fluid Mechanics*. 7th ed. Hoboken, NJ: John Wiley & Sons.

Owen A (2007) *The application of low aspect ratio hydrofoils to the secure positioning of static equipment in tidal streams*. PhD Thesis, The Robert Gordon University. Available at: https://openair.rgu.ac.uk/handle/10059/470 (accessed 17 December 2013).

Ocean SI (2013) Ocean energy: cost of energy and cost reduction opportunities, strategic initiative for ocean energy. Available at: http://oceanenergy-sweden.se/wp-content/uploads/2018/03/130501-si-ocean-cost-of-energy-report.pdf (accessed 7 June 2018).

Sustainable Energy Ireland (2007) SEI, tidal & current energy resources in Ireland, sustainable energy authority of Ireland. Available at: https://www.seai.ie/resources/publications/Tidal_Current_Energy_Resources_in_Ireland_Report.pdf (accessed 25 May 2017).

The Carbon Trust (2011) Accelerating Marine Energy. The potential for cost reduction – Insights from the carbon trust marine energy accelerator. Available at: http://www.carbon-trust.com/media/5675/ctc797.pdf (accessed 25 May 2017).

Thompson D and Beasley DJ (eds) (2012) Handbook for Marine Geotechnical Engineering SP-2209-OCN. Port Hueneme, CA: Naval Facilities Engineering Command. Available at: http://www.dtic.mil/dtic/tr/fulltext/u2/a556807.pdf (accessed 14 June 2018).

TidalEnergyToday(2015)Estimateofglobalpotentialtidalresources. Available at: http://tidalenergytoday.com/2015/02/17/estimate-of-global-potential-tidal-resources/ on (accessed 25 May 2017).

United Kingdom Department for Business, Energy & Industrial Strategy (2017) Quarterly energy prices. Available at: http://www.gov.uk/government/uploads/system/uploads/attachment_data/file/604131/QEP_Q416.pdf (accessed 25 May 2017).

Author biographies

Gerry Byrne is a Senior Experimental Officer in the Fluids & Heat Transfer research group, Department of Mechanical & Manufacturing Engineering at Trinity College Dublin. Mr. Byrne has co-authored more than 10 publications related to heat transfer, fluid mechanics in the field of sustainable energy. He holds a Postgraduate Diploma in Renewable Energy from Trinity College Dublin and is an Association of Energy Engineers Certified Measurement and Verification Professional.

Tim Persoons is an Assistant Professor in Mechanical Engineering at Trinity College Dublin and Visiting Faculty at Purdue University. He has co-authored more than 100 journal and conference publications in experimental and computational fluid mechanics and heat transfer, covering topics in multi-scale electronics cooling and flow control. He is an Associate Editor for IEEE Transactions for Components, Packaging and Manufacturing Technology, Therminic scientific committee member and co-recipient of the 2013 ICHMT Hartnett-Irvine Award.

William Kingston is an Adjunct Professor in the School of Business at Trinity College Dublin. He has coauthored 75 peer-reviewed publications as well as several patents related to tidal energy devices, including their positioning and anchoring.

Appendix I

Notation

α	angle-of-attack (°)
A	area (m²)
AR	aspect ratio, $AR = b/c$ (−)
b	wingspan (m)
c	chord length (m)
C_l, C_d	lift and drag coefficients
D	immersion depth (m)
F	force (N)
h	camber (m)
N_{crit}	critical transition number in Xfoil (−)
p	Pence (=0.01 Great Britain Pound Sterling)
Re	Reynolds number (−)
SF	safety factor (−)

t	thickness (m)
U	flow velocity (m/s)
μ	friction coefficient (–)
ρ	density (kg/m³)

Appendix 2

Measurement uncertainty analysis

The lift and drag sensor measurement uncertainty has been determined based on the standard deviation of the signal voltages during the measurement, averaged over 4-second intervals. A confidence level of 95% is assumed and the distribution is assumed Gaussian. The lift force sensor has an estimated uncertainty margin of ± 5.1 kg-force (e.g. a lift force of 144($\pm$3.2%) kg-force at an angle-of-attack of 3°).

Initially, the drag force sensor had an estimated uncertainty margin of only ± 1.0 kg (e.g. a drag force of 35($\pm$2.6%) kg-force at an angle-of-attack of 3°). However, before the start of the higher angle-of-attack measurements (at 8° and 11.4°), the drag sensor reading exhibited an intermittent failure, alternating between reading correct values and not responding. This increased the uncertainty margin in the final two tests to a much higher value, averaging at $\pm 13\%$.

For the flow velocity, the ADCP probe was available only for the final two measurements (at 8° and 11.4°). Its reading has an estimated uncertainty of approximately $\pm 2\%$ (e.g. 2.11 ± 0.04 m/s for the measurement with the hydrofoil at an angle-of-attack of 8°). The earlier measurements are based on a combination of the pitot static probe and optical surface flow velocity measurements, with a higher uncertainty margin estimated at ± 0.25 m/s .

Appendix 3

Mechanical strength analysis of the test apparatus

A finite element analysis (FEA) was carried out on the hydrofoil test apparatus, with loads applied to represent the worst-case scenario forces corresponding to a 4-m/s water flow through the sluice. The vertical, downward lift force is distributed equally (50/50) over both arms, yet the horizontal, streamwise drag force is distributed unequally (70% on one arm and 30% on the other), to test the effect of twisting torque on the rig. It should be noted that this situation is not expected to occur, since the rig is mounted in the middle of the sluice where the approaching flow velocity is reasonably left/right symmetric. Table 2 summarises the structural characteristics of the apparatus.

Table 2. Summary of mechanical strength analysis of hydrofoil test apparatus.

Quantity	Streamwise	Cross-stream
Maximum expected force[a]	2300 N	4200 N
Maximum deflection at hydrofoil	1.5 mm	1.8 mm
Maximum mechanical stress	27 MPa	25 MPa
Safety factor	10	11
Mechanical stiffness	1.53 kN/mm	2.33 kN/mm
Equivalent resonant mass	100 kg	100 kg
Resonance frequency	19.7 Hz	24.3 Hz

[a]Estimated values for a flow velocity of 4 m/s.